Electronic Supplementary Information for

Surface and Optical Properties of Phase-Pure Silver Iodobismuthate Nanocrystals

Anastasia Matuhina,[a] G. Krishnamurthy Grandhi,[a] Ashanti Bergonzoni,[b] Laurent Pedesseau,[b] Roberto Grisorio,[c] Shambhavee Annurakshita,[d] Harri Ali-Löytty,[e] Riya Varghese,[d] Kimmo Lahtonen,[f] George Volonakis,[g] Vincenzo Pecunia,[h] Godofredo Bautista,[d] Jacky Even[b], and Paola Vivo,*[a]

[a] *Hybrid Solar Cells, Faculty of Engineering and Natural Sciences, Tampere University, P.O. Box 541, FI-33014 Tampere University, Finland*
**Email: paola.vivo@tuni.fi*
[b] *Univ Rennes, INSA Rennes, CNRS, Institut FOTON – UMR 6082, F-35000 Rennes, France*
[c] *Dipartimento di Ingegneria Civile, Ambientale, del Territorio, Edile e di Chimica (DICATECh), Politecnico di Bari, Via Orabona 4, 70125 Bari, Italy*
[d] *Photonics Laboratory, Physics Unit, Faculty of Engineering and Natural Sciences, Tampere University, FI-33014 Tampere, Finlande*
[e] *Surface Science Group, Photonics Laboratory, Tampere University, P.O. Box 692, FI-33014 Tampere University, Finland*
[f] *Faculty of Engineering and Natural Sciences, Tampere University, P.O. Box 692, Tampere FI-33014, Finland*
[g] *Univ Rennes, ENSCR, INSA Rennes, CNRS, ISCR (Institut des Sciences Chimiques de Rennes), UMR 6226, 35700 Rennes, France.*
[h] *School of Sustainable Energy Engineering, Simon Fraser University, 5118 – 10285 University Drive, Surrey, British Columbia V3T 0N1, Canada*

Contents

Synthesis of the $AgBiI_4$ NCs. 2
Details of the Density-functional (DFT) theory 2
Computational details 2
Modeling the bulk $AgBiI_4$ 3
Design of the nanoplatelets 4
Synthesis optimization 5
XRD pattern 6
Structural parameters 6
XPS survey scan 7
TEM images 8
SEM image 8
Thermal stability 9
DFT electronic band structure calculations 10
Optical band gap values of $AgBiI_4$ 13
References 14

Synthesis of the $AgBiI_4$ NCs.

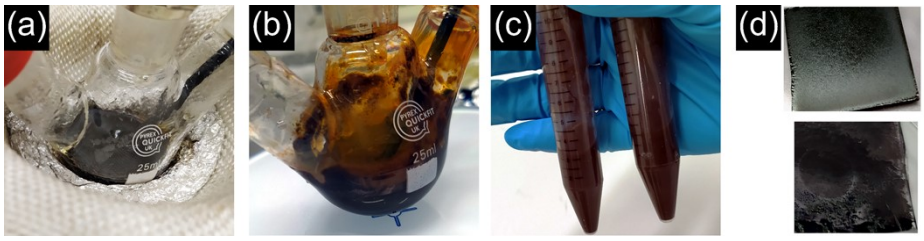

Fig. S1. Hot-injection synthesis of the $AgBiI_4$ NCs. (a)AgBi precursor solution before the TMS-I injection. (b) $AgBiI_4$ NCs after cooling down to the room temperature. (c) Purified $AgBiI_4$ NCs redispersed in the hexane. (d) drop casted NC films. Top side – before the anti-solvent washing, bottom side – after the anti-solvent washing.

Details of the Density-functional (DFT) theory

Computational details

First, DFT calculations were performed mainly using the SIESTA code based on a basis set of finite-range of numerical atomic orbitals[1,2] as it enables to treat large slabs at relatively low computational cost. A real space mesh grid energy cutoff 300 Ry with the polarized double basis set with an energy shift of 100 meV were defined. The reciprocal space of the bulk and slab systems were sampled with a Monkhorst-Pack grid[3,4] of 6x6x2 and 6x6x1, respectively. The structural relaxations, when carried, were done with the fast inertial relaxation engine (FIRE) algorithm[5] with the force tolerance set to 0.02 eV/A. It was then associated with Van Der Waals density functional with C09 correction within the van der Waals DF2 flavor to describe the exchange-correlation term.[6] Single point calculations were performed with PBE functional on top of the optimized structures when relevant. Spin-orbit coupling (SOC) was considered in its off-site approximation when used.[7,8]

Comment [MG(]: 1. Soler, J. M *J. Phys. Condens. Matter* **2002**, *14* (11), 2745–2779. https://doi.org/10.1088/0953-8984/14/11/302. 2. García, A. *J. Chem. Phys.* **2020**, *152* (20), 204108. https://doi.org/10.1063/5.0005077)

Comment [MG(]: (https://doi.org/10.1103/PhysRevB.16.1748. https://doi.org/10.1103/PhysRevB.13.5188.)

Comment [MG(]: (Bitzek, E. *Phys. Rev. Lett.* **2006**, *97* (17), 170201. https://doi.org/10.1103/PhysRevLett.97.170201.)

Comment [MG(]: (Cooper, V. R. *Phys. Rev. B* **2010**, *81* (16), 161104. https://doi.org/10.1103/PhysRevB.81.161104.)

Comment [MG(]: (Perdew, J. P. *Phys. Rev. Lett.* **1996**, *77* (18), 3865–3868. https://doi.org/10.1103/PhysRevLett.77.3865)

Comment [MG(]: (Cuadrado, R.; *J. Phys. Condens. Matter* **2012**, *24* (8), 086005. https://doi.org/10.1088/0953-8984/24/8/086005. Cuadrado, R. *Catal. React.* **2017**, 45.)

Second, as a benchmark, some single point or electronic band calculations were also performed with Quantum Espresso (QE) or with VASP plane-wave codes.[9–11,11,12] In QE, norm-conserving fully relativistic PBE pseudopotentials[13] were used together with an 80 Ry cutoff for the plane-wave kinetic energy and a converged 8×8×8 Brillouin zone sampling.

In VASP, for electronic structure calculation, density functional theory (DFT) calculations are performed using the plane-wave projector augmented wave (PAW) method as implemented in the VASP code.[14,15] We used the PAW data set supplied in the VASP package with the following valence orbitals: Ag [$4d^{10}5s^{1}$], Bi [$6s^{2}6p^{3}$], and I [$5s^{2}5p^{5}$] atoms. In addition, the wavefunctions are expanded using a plane-wave basis set with an energy cut-off of 550 eV. Subsequent calculations to determine electronic band structures are performed using two different levels of theory (i) PBE with the addition of spin-orbit coupling (PBE+SOC) and (ii) the Heyd, Scuseria and Ernzerhof (HSE) hybrid functional with SOC (HSE+SOC).[16–19] For reciprocal space integration, 4x4x2 (Bulk) and 2x2x1 (Slab) Monkhorst-Pack grids were used for all cells described below. For convergence purposes, we used at least 70 and up to 90 conduction bands.

Modeling the bulk $AgBiI_4$

The complexity of the $AgBiI_4$ crystal structure, due to occupational-site disorder at the positions of Ag and Bi atoms, makes it particularly challenging to model. Previous studies [20–22] have proposed different models to best mimic the properties of the bulk compound. Herein, we employed the model proposed by Cucco et al[23] as it effectively reproduces the measured XRD pattern and band gap. Derived from Wyckoff position splitting of the Fd3m parent structure, the model structure is described within the *Imma* space group with Ag atoms occupying 4a sites and Bi 4d ones.

To assess the reliability of the atomic orbital-based Siesta code in reproducing the electronic properties of $AgBiI_4$, we calculated the band structure of the Imma ideal model at

Comment [MG(]: (Giannozzi, P. *J. Phys. Condens. Matter* **2017**, *29* (46), 465901. https://doi.org/10.1088/1361-648X/aa8f79. Giannozzi, P. *J. Phys. Condens. Matter* **2009**, *21* (39), 395502. https://doi.org/10.1088/0953-8984/21/39/395502.)

Comment [MG(]: (https://doi.org/10.1016/0927-0256(96)00008-0. https://doi.org/10.1103/PhysRevB.54.11169. https://doi.org/10.1103/PhysRevB.74.035101.)

Comment [MG(]: (van Setten, M. J. *Comput. Phys. Commun.* **2018**, *226*, 39–54. https://doi.org/10.1016/j.cpc.2018.01.012)

Comment [MG(]: (https://doi.org/10.1063/1.2187006. https://doi.org/10.1063/1.1564060. https://doi.org/10.1063/1.1760074. https://doi.org/10.1063/1.2204597.)

Comment [MG(]: (Barone, V. T https://doi.org/10.1063/5.0088980. Danilović, D. https://doi.org/10.1021/acs.jpcc.2c03208.)

the PBE and PBE + SOC level of theories and compared it the QE resulting ones (**Figure S8**). At the same level of theory, Siesta demonstrated good agreement with plane-wave computed band structures features. Namely, we observed similar bands shapes and bang gaps (0.45 VS 0.52 eV at PBE+SOC level), with a VBM at Γ and a CBM nearly degenerated between Γ and R. Noteworthy to mention the known band gap underestimation given by the PBE functional. QE results further allowed us to identify the wavefunctions symmetries of the VBM and CBM at Γ and R. The results of this symmetry analysis are reported in Table S4.

Anticipating the surface study, the cell parameters and the atomic positions of the ideal Imma structure have been relaxed under the constraint of an orthorhombic cell using Siesta. This resulted in a small volume contraction of around 1% and a narrowing of 0.04 eV of the band gap (**Figure S9a**).

Design of the nanoplatelets

We designed the (001)-BiI and (001)-AgI terminated slabs by constructing supercells size along the [001] direction of the *Imma* conventional cell. These surfaces are simply referred as BiI and AgI thereafter. The Siesta optimized bulk structure was used as a starting point and the atomic positions constituting the outermost 2 octahedra layers were relaxed. A vacuum as large as 100 Å was used to avoid spurious interactions between periodic images. To be able to run HSE calculation for the surface study, we considered a thin (36 Å) and a thicker (60 Å) well thickness corresponding to 6 and 10 layers of octahedra respectively. For computational cost reasons, only the smallest one was considered for the HSE calculations with a vacuum thickness of 30 Å. Furthermore, having different slab thicknesses provided insight into the effect of the quantum confinement on the electronic band gap (**Figure S10**). It was found to be quite weak, further confirming our experimental and theoretical findings, and in line with the results of Danilović et al.[22]

Comment [MG(]: (Danilović, D. *J. Phys. Chem. C* **2022**, *126* (32), 13739–13747. https://doi.org/10.1021/acs.jpcc.2c03208 .)

Synthesis optimization

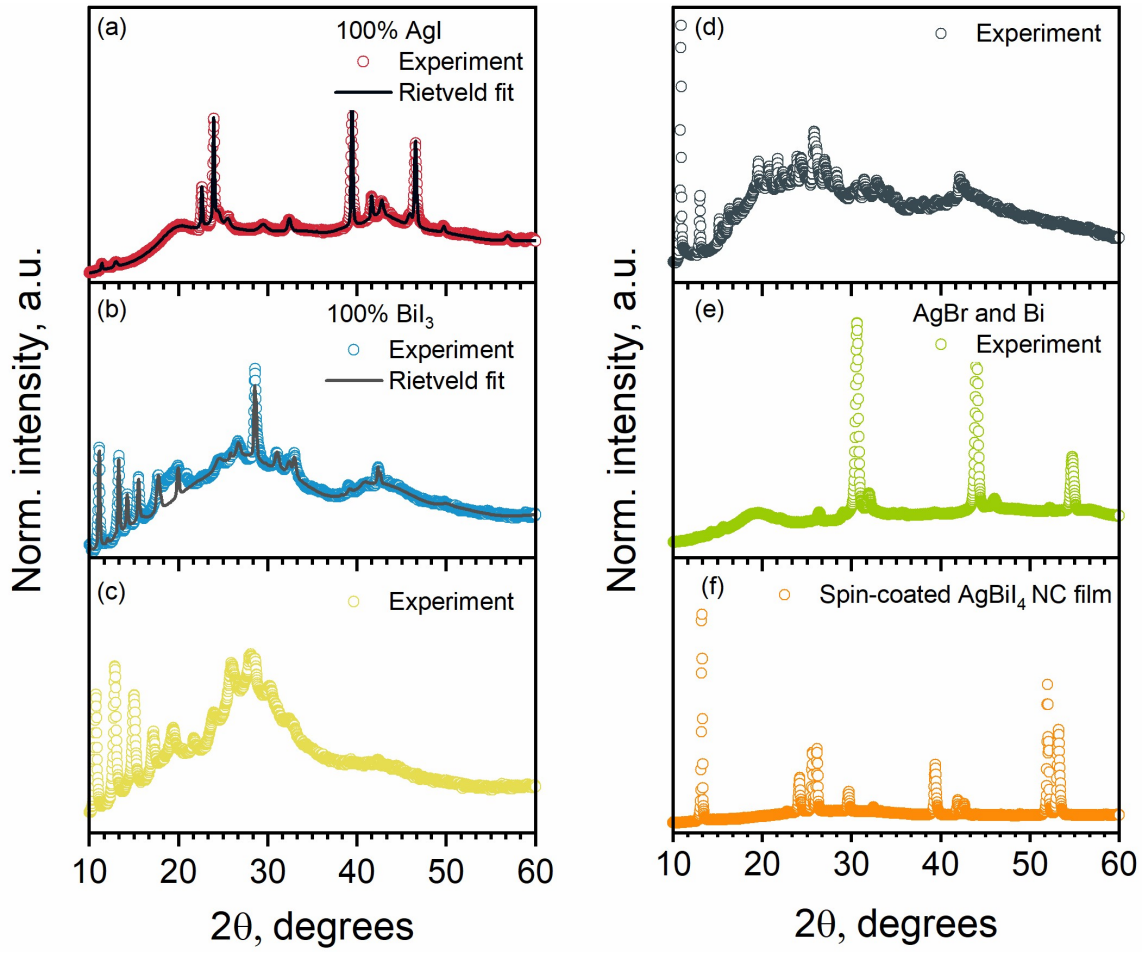

Figure S2. XRD patterns of the NCs obtained during the synthesis optimization. (a) Synthesis below 190°C. (b) Synthesis with decreased ligand ratio. (c) Synthesis with 4 times lower precursor concentration of metal acetates and TMS-I. (d) Synthesis with increased amount of TMS-I to 2 times. (e) Synthesis of the $AgBiBr_4$ counterpart. (f) Spin-coated $AgBiI_4$ NC film.

XRD pattern

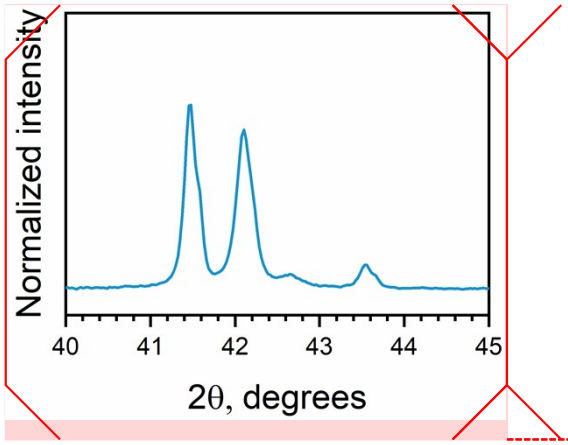

Figure S3. The XRD pattern of $AgBiI_4$ NCs in the 40°–45° range.

Structural parameters

Table S1. Lattice Parameters obtained by Rietveld Refinement of the Experimental XRD Patterns and Rietveld refined structural parameters of $AgBiI_4$ NCs.

Space group	*a* (Å)	*b* (Å)	*c* (Å)	*V* (Å)^3	R_{wp} (%)	χ^2
Fd-3m	12.0917	12.0917	12.0917	1767.919	3.86	4.99

Atom	Wyckoff position	Occupancy (g)	*x*	*y*	*z*
Bi	16c	0.5495	0	0	0
I	32e	1.0000	0.264691	0.264691	0.264691
Ag	16c	0.3513	0	0	0

Comment [MG(]: @Anastasia, Harri's comment about minor ticks is: the number of minor ticks should be '4' instead of '5'

Comment [AM(]: Fixed

XPS survey scan

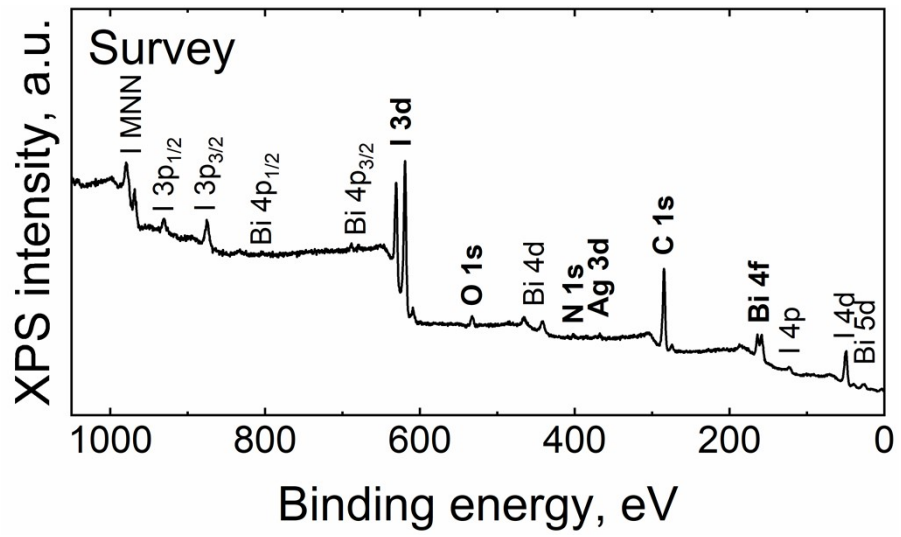

Figure S4. XPS survey spectrum for $AgBiI_4$ NC film samples.

TEM images

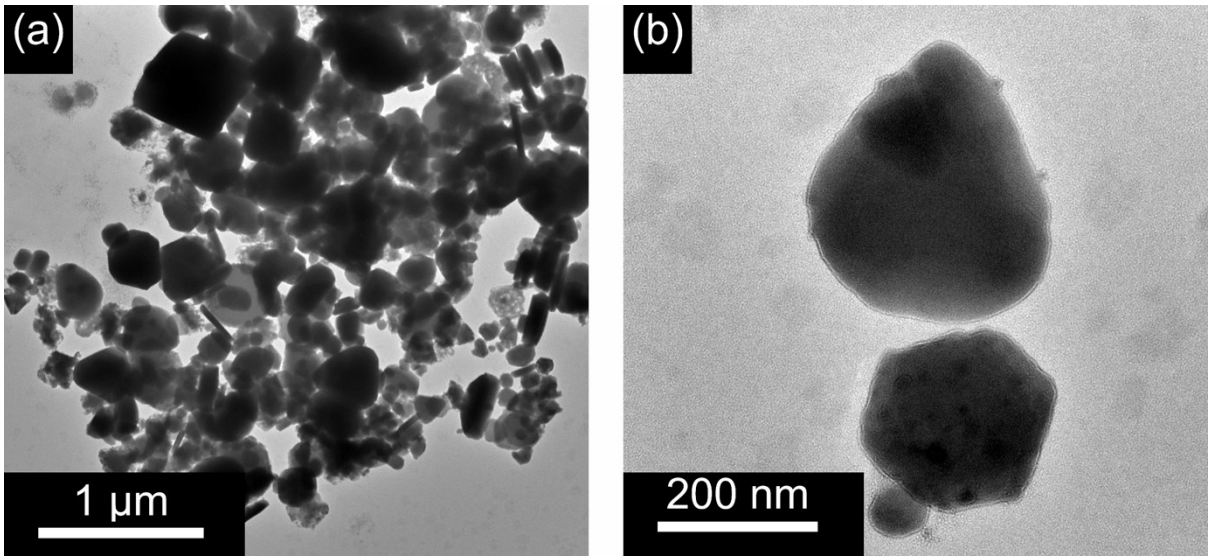

Figure S5. (a) Low and (b) high-magnification TEM images of $AgBiI_4$ NCs.

SEM image

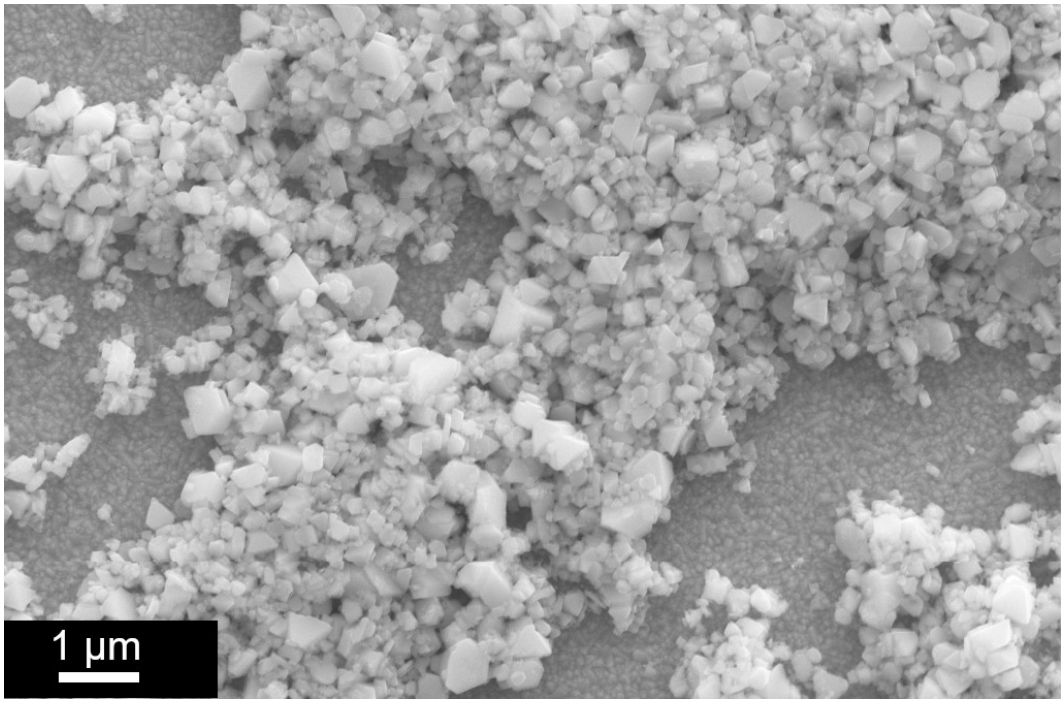

Figure S6. SEM image of the spin coated $AgBiI_4$ NC film.

Thermal stability

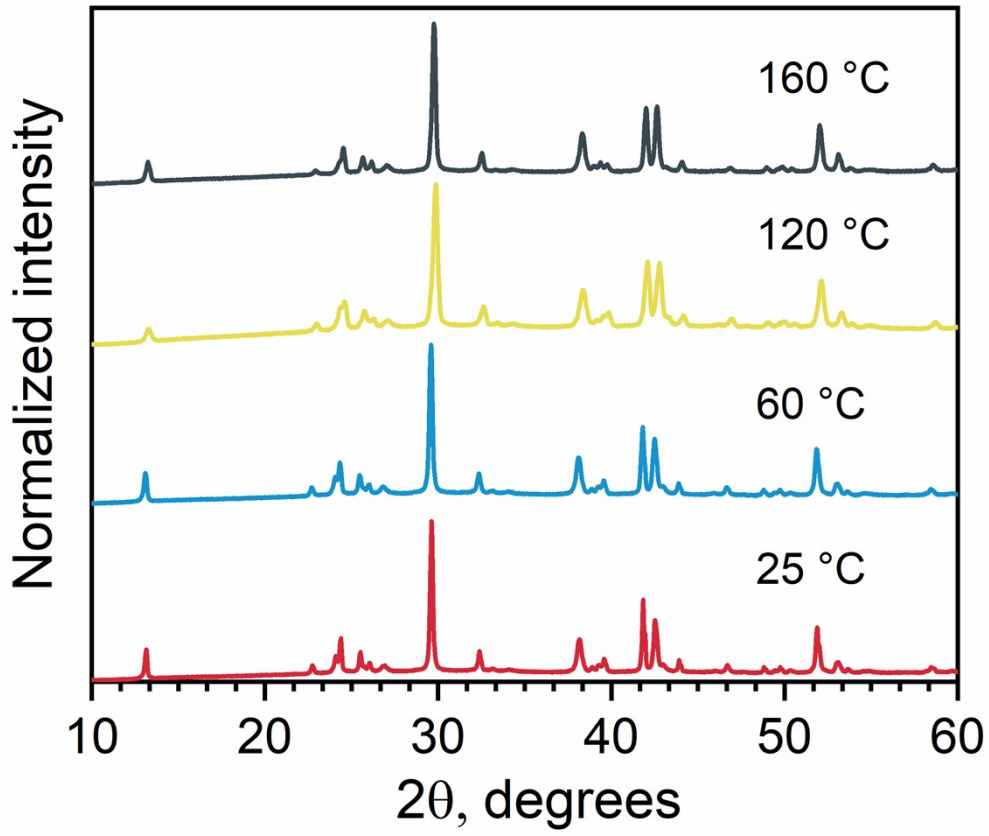

Figure S7. Room temperature XRD patterns of $AgBiI_4$ NC films pre-annealed at different temperatures for 10 min in the air.

DFT electronic band structure calculations

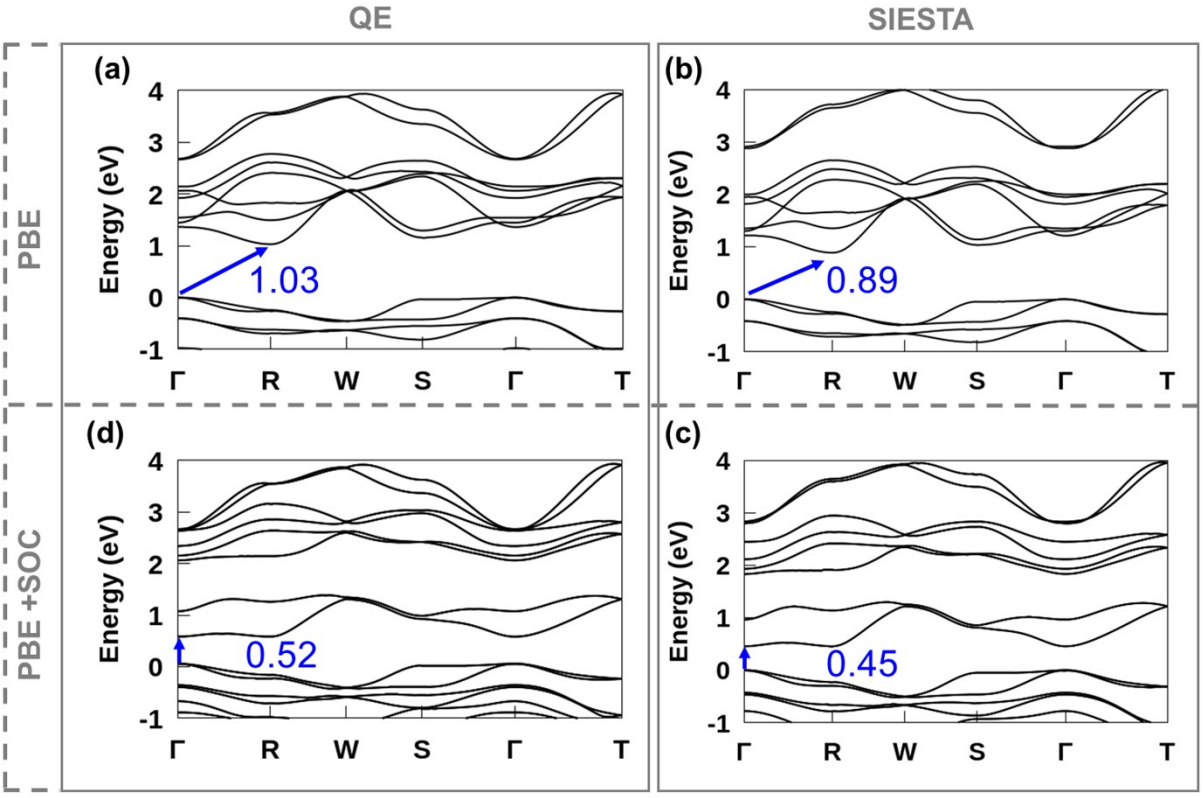

Figure S8. Comparison between the electronic band structure computed with QE (left) and Siesta (right) at PBE (top) and PBE+SOC (bottom) levels.

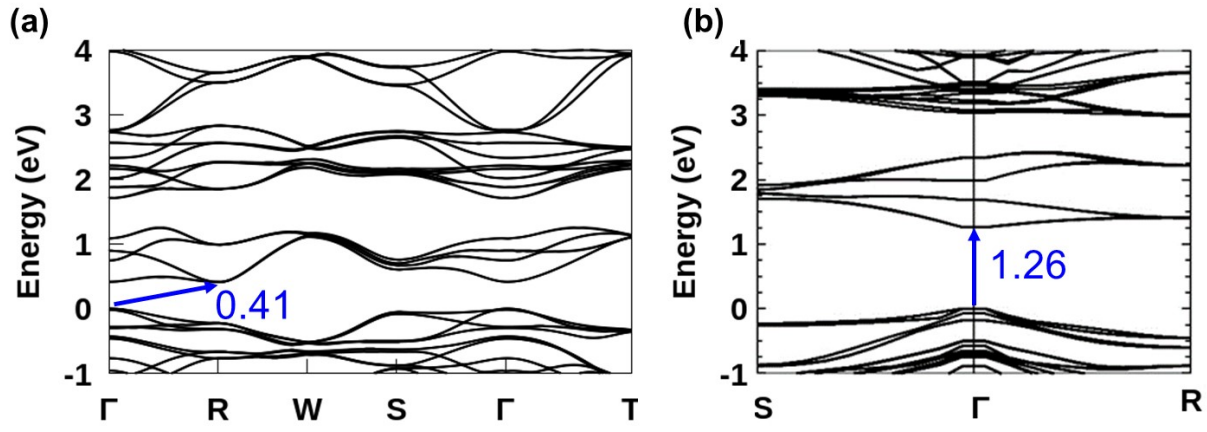

Figure S9. Electronic band structures of the bulk optimized structure computed (a) with siesta at the PBE+SOC level and (b) HSE corrected with VASP.

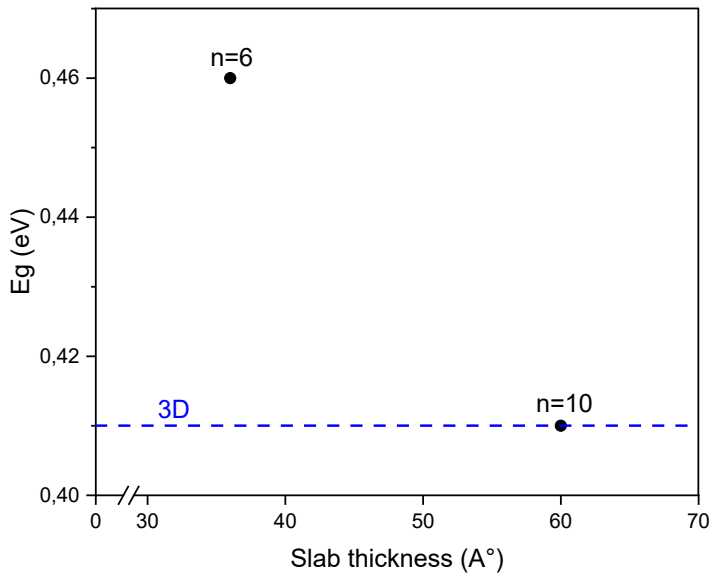

Figure S10. Evolution of the calculated band gap as function of the slab thickness. NCs with sizes on the order of hundreds of nanometers should not exhibit significant quantum confinement effect.

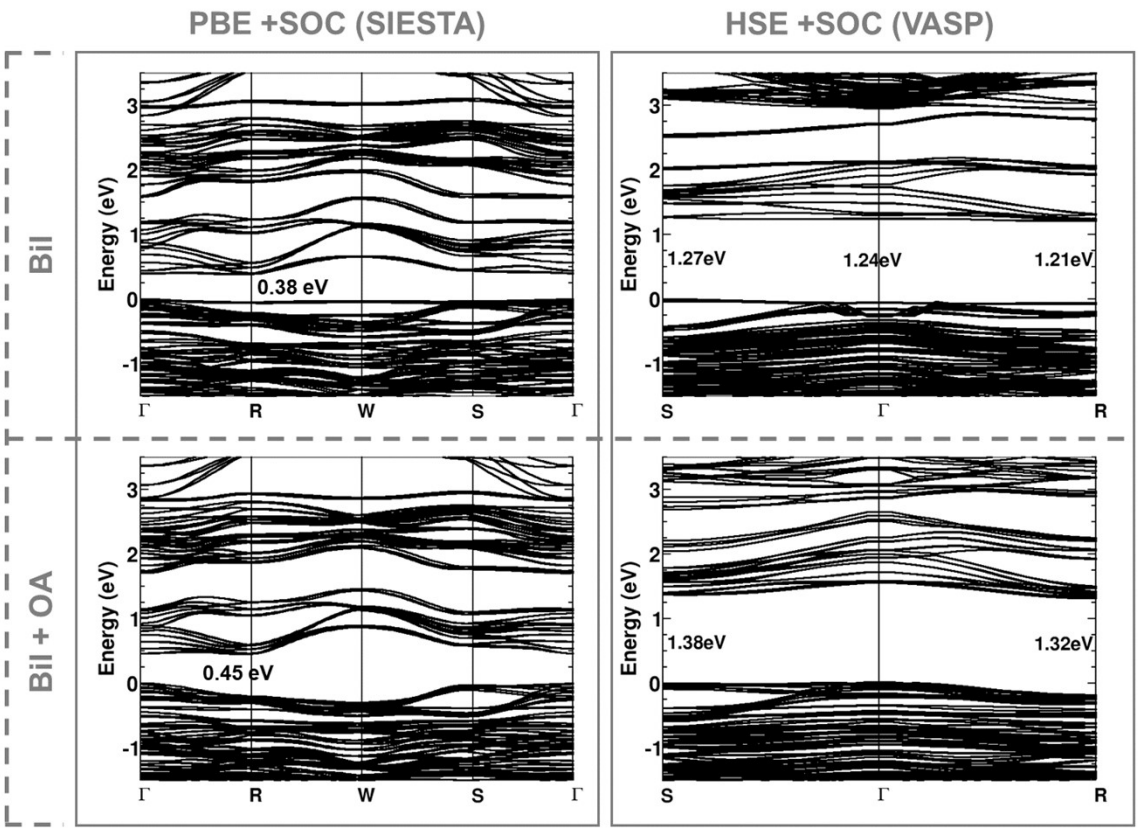

Figure S11. Comparison between the PBE+SOC (siesta, left) and HSE-corrected (VASP, right) band structures of the small slab without (top) and with (bottom) OA coating.

Optical band gap values of $AgBiI_4$

Table S2. Reported direct and indirect band gap values of $AgBiI_4$.

Compound	Direct band gap, eV	In-direct band gap, eV	Reference
$AgBiI_4$	1.78	1.6	[24]
$AgBiI_4$	1.63	1.55	[25]
$AgBiI_4$	1.78	-	[26]
$AgBiI_4$	1.93	-	[27]
$AgBiI_4$	1.73	1.63	[28]
$AgBiI_4$	1.8	1.75	[28]
$AgBiI_4$	1.78	1.73	[28]
$AgBiI_4$	1.73	-	[29]
$AgBiI_4$	1.79	1.73	This work

Table S3. Symmetry analysis of direct optical transitions from the VBM and CBM of $AgBiI_4$ described in the *Imma* space group.

High symmetry point	Γ (C_{2h})	R (C_i)
IR (r)	$A_u + B_u$	$3*A_u$
With out SOC		
IR (φ_i)	B_g	A_g
IR (φ_f)	B_u	A_u
Direct product	A_u → allowed	A_u → allowed
With SOC		
IR (φ_i)	$^1E_{1/2g} + {}^2E_{1/2g}$	$A_{1/2g}$
IR (φ_f)	$^1E_{1/2u} + {}^2E_{1/2u}$	$A_{1/2u}$
Direct product	$2*A_u + 2*$→ allowed	A_u → allowed

References

1 J. M. Soler, E. Artacho, J. D. Gale, A. García, J. Junquera, P. Ordejón and D. Sánchez-Portal, *J. Phys. Condens. Matter*, 2002, **14**, 2745.

2 A. García, N. Papior, A. Akhtar, E. Artacho, V. Blum, E. Bosoni, P. Brandimarte, M. Brandbyge, J. I. Cerdá, F. Corsetti, R. Cuadrado, V. Dikan, J. Ferrer, J. Gale, P. García-Fernández, V. M. García-Suárez, S. García, G. Huhs, S. Illera, R. Korytár, P. Koval, I. Lebedeva, L. Lin, P. López-Tarifa, S. G. Mayo, S. Mohr, P. Ordejón, A. Postnikov, Y. Pouillon, M. Pruneda, R. Robles, D. Sánchez-Portal, J. M. Soler, R. Ullah, V. W. Yu and J. Junquera, *J. Chem. Phys.*, 2020, **152**, 204108.

3 H. J. Monkhorst and J. D. Pack, *Phys. Rev. B*, 1976, **13**, 5188–5192.

4 J. D. Pack and H. J. Monkhorst, *Phys. Rev. B*, 1977, **16**, 1748–1749.

5 E. Bitzek, P. Koskinen, F. Gähler, M. Moseler and P. Gumbsch, *Phys. Rev. Lett.*, 2006, **97**, 170201.

6 V. R. Cooper, *Phys. Rev. B*, 2010, **81**, 161104.

7 J. P. Perdew, K. Burke and M. Ernzerhof, *Phys. Rev. Lett.*, 1996, **77**, 3865–3868.
8 R. Cuadrado and J. I. Cerdá, *J. Phys. Condens. Matter*, 2012, **24**, 086005.
9 P. Giannozzi, O. Andreussi, T. Brumme, O. Bunau, M. B. Nardelli, M. Calandra, R. Car, C. Cavazzoni, D. Ceresoli, M. Cococcioni, N. Colonna, I. Carnimeo, A. D. Corso, S. de Gironcoli, P. Delugas, R. A. DiStasio, A. Ferretti, A. Floris, G. Fratesi, G. Fugallo, R. Gebauer, U. Gerstmann, F. Giustino, T. Gorni, J. Jia, M. Kawamura, H.-Y. Ko, A. Kokalj, E. Küçükbenli, M. Lazzeri, M. Marsili, N. Marzari, F. Mauri, N. L. Nguyen, H.-V. Nguyen, A. Otero-de-la-Roza, L. Paulatto, S. Poncé, D. Rocca, R. Sabatini, B. Santra, M. Schlipf, A. P. Seitsonen, A. Smogunov, I. Timrov, T. Thonhauser, P. Umari, N. Vast, X. Wu and S. Baroni, *J. Phys. Condens. Matter*, 2017, **29**, 465901.
10 P. Giannozzi, S. Baroni, N. Bonini, M. Calandra, R. Car, C. Cavazzoni, D. Ceresoli, G. L. Chiarotti, M. Cococcioni, I. Dabo, A. D. Corso, S. de Gironcoli, S. Fabris, G. Fratesi, R. Gebauer, U. Gerstmann, C. Gougoussis, A. Kokalj, M. Lazzeri, L. Martin-Samos, N. Marzari, F. Mauri, R. Mazzarello, S. Paolini, A. Pasquarello, L. Paulatto, C. Sbraccia, S. Scandolo, G. Sclauzero, A. P. Seitsonen, A. Smogunov, P. Umari and R. M. Wentzcovitch, *J. Phys. Condens. Matter*, 2009, **21**, 395502.
11 G. Kresse and J. Furthmüller, *Comput. Mater. Sci.*, 1996, **6**, 15–50.
12 M. Shishkin and G. Kresse, *Phys. Rev. B*, 2006, **74**, 035101.
13 M. J. van Setten, M. Giantomassi, E. Bousquet, M. J. Verstraete, D. R. Hamann, X. Gonze and G.-M. Rignanese, *Comput. Phys. Commun.*, 2018, **226**, 39–54.
14 P. E. Blöchl, *Phys. Rev. B*, 1994, **50**, 17953–17979.
15 G. Kresse and D. Joubert, *Phys. Rev. B*, 1999, **59**, 1758–1775.
16 J. Paier, M. Marsman, K. Hummer, G. Kresse, I. C. Gerber and J. G. Ángyán, *J. Chem. Phys.*, 2006, **124**, 154709.
17 J. Heyd, G. E. Scuseria and M. Ernzerhof, *J. Chem. Phys.*, 2003, **118**, 8207–8215.
18 J. Heyd and G. E. Scuseria, *J. Chem. Phys.*, 2004, **121**, 1187–1192.
19 J. Heyd, G. E. Scuseria and M. Ernzerhof, *J. Chem. Phys.*, 2006, **124**, 219906.
20 V. T. Barone, B. R. Tuttle and S. V. Khare, *J. Appl. Phys.*, 2022, **131**, 245701.
21 D. Danilović, A. R. Milosavljević, P. Sapkota, R. Dojčilović, D. Tošić, N. Vukmirović, M. Jocić, V. Djoković, S. Ptasinska and D. K. Božanić, *J. Phys. Chem. C*, 2022, **126**, 13739–13747.
22 D. Danilović, A. R. Milosavljević, P. Sapkota, R. Dojčilović, D. Tošić, N. Vukmirović, M. Jocić, V. Djoković, S. Ptasinska and D. K. Božanić, *J. Phys. Chem. C*, 2022, **126**, 13739–13747.
23 B. Cucco, L. Pedesseau, C. Katan, J. Even, M. Kepenekian and G. Volonakis, .
24 H. Zhu, M. Pan, M. B. Johansson and E. M. J. Johansson, *ChemSusChem*, 2017, **10**, 2592–2596.
25 M. D. Prasad, M. G. Krishna and S. K. Batabyal, *ACS Appl. Nano Mater.*, 2021, **4**, 1252–1259.
26 I. Turkevych, S. Kazaoui, E. Ito, T. Urano, K. Yamada, H. Tomiyasu, H. Yamagishi, M. Kondo and S. Aramaki, *ChemSusChem*, 2017, **10**, 3754–3759.
27 A. Bera, S. Paramanik, A. Maiti and A. J. Pal, *Phys. Rev. Mater.*, 2021, **5**, 1–8.
28 H. C. Sansom, G. F. S. Whitehead, M. S. Dyer, M. Zanella, T. D. Manning, M. J. Pitcher, T. J. Whittles, V. R. Dhanak, J. Alaria, J. B. Claridge and M. J. Rosseinsky, *Chem. Mater.*, 2017, **29**, 1538–1549.
29 N. Pai, J. Lu, T. R. Gengenbach, A. Seeber, A. S. R. Chesman, L. Jiang, D. C. Senevirathna, P. C. Andrews, U. Bach, Y. Cheng and A. N. Simonov, 2019, **1803396**, 1–11.